Supporting Information for

Terminal-fluoride-coordinated air-stable chiral dysprosium single-molecule magnets

Jinjiang Wu,[a,c] Guo-Lu Wang,[b] Zhenhua Zhu,[a,d] Chen Zhao,[a,c] Xiao-Lei Li,[a] Yi-Quan Zhang*[b] and Jinkui Tang*[a,c]

[a] State Key Laboratory of Rare Earth Resource Utilization, Changchun Institute of Applied Chemistry, Chinese Academy of Sciences, Changchun 130022, P. R. China
[b] Jiangsu Key Lab for NSLSCS, School of Physical Science and Technology, Nanjing Normal University, Nanjing 210023, P. R. China
[c] School of Applied Chemistry and Engineering, University of Science and Technology of China, Hefei 230026, P. R. China
[d] University of Chinese Academy of Sciences, Beijing 100049, P.R. China

Synthesis and characterization

General procedure

All coordination reaction manipulations describe below were performed under aerobic conditions. (1*R*,2*R*)-1,2-di-*o*-tolylethane-1,2-diamine and (1*S*,2*S*)-1,2-di-*o*-tolylethane-1,2-diamine were synthesized according to the published procedure.[1] Other chemicals were purchased from commercial sources and used as received without any further purification.

Measurements

FT-IR spectra were recorded on a Nicolet 6700 Flex FTIR spectrometer equipped with a smart iTR attenuated total reflectance (ATR) sampling accessory in the range from 4000-540 cm^{-1}. CD spectra data were collected on a Jasco J-820 spectropolarimeter at room temperature with scanning speed of 200 nm/min and bandwidth of 5 nm. Thermogravimetric analyses (TGA) were completed using a Netzsch STA449F3 TG-DSC instrument in the range of 30-800 ºC with a heating rate of 10 K min^{-1} under N_2 atmosphere. X-ray photoelectron spectra (XPS) were taken using a Thermo ESCALAB 250 photoelectron spectrometer. Single crystal X-ray diffraction measurements were performed on a Bruker Apex II CCD diffractometer with graphite-monochromated Mo Kα radiation (λ = 0.71073 Å) at 180 K. The structures were solved by direct methods using SHELXT[2] and refined by full-matrix least-squares methods with SHELXL[3] on F^2 with anisotropic thermal parameters for all non-hydrogen atoms in the Olex2 package.[4] The hydrogen atoms were introduced in calculated positions and refined with a fixed geometry with respected to their carrier atoms. Powder X-ray diffraction measurement were recorded on Bruker D8 advance X-ray diffractometer using Cu-Kα

radiation. All magnetic susceptibility measurements were carried on a Quantum Design MPMS-XL7 magnetometer equipped with a 7 T magnet. Direct-current (dc) magnetic susceptibility measurements were performed at the temperature range from 2 to 300 K with an external magnetic field of 1000 Oe. Alternative-current (ac) magnetic susceptibility data were collected in zero applied field with a 3.0 Oe ac oscillating field in the temperature range 2-30 K. The experimental magnetic susceptibility data were corrected for the diamagnetism estimated from Pascal's constants and sample holder calibration.

Synthesis

Synthesis procedure for **1**

(1S,2S)-1,2-di-o-tolylethane-1,2-diamine (48.1 mg, 0.2 mmol) and pyridine-2,6-dicarbaldehyde (27.0 mg, 0.2 mmol) were dissolved in methanol, followed by addition of $DyCl_3 \cdot 6H_2O$ (37.7 mg, 0.1 mmol). The mixture was stirred and reflexed for 12 h. Then, methanol was evaporated under reduced pressure, yielding orange powders. The obtained orange powder and sodium tetraphenylboron (34.2 mg, 0.1 mmol) was added to a solution of NaF (0.6 mmol, 25.2 mg) in 2 ml H_2O and 16 ml MeOH, which was stirred at room temperature for 3h, resulting a turbid liquid. Then, the mixture was filtered and left unperturbed to allow the slow evaporation of the solvent. The light-yellow crystals suitable for X-ray diffraction were obtained after several days. (28 mg, 22%, based on Dy) FTIR υ/cm^{-1} (ART): 528.00(m), 584.91(m), 613.08(m), 702.43(s), 729.78(s), 757.32(m), 805.66(s), 848.42(w), 970.46(w), 1009.92(s), 1032.44(m), 1058.94(w), 1098.69(w), 1162.75 (s), 1270.05(m), 1380.73(w), 1426.52(m), 1461.33(s), 1478.50(m), 1591.33(s), 1650.49(m), 3052.35(w).

Synthesis procedure for **2**

Compound **2** was synthesized in a similar fashion to **1** except that (1R,2R)-1,2-di-o-tolylethane-1,2-diamine was used instead of (1S,2S)-1,2-di-o-tolylethane-1,2-diamine. (30 mg, 23%, based on Dy) FTIR υ/cm^{-1} (ART): 529.81(m), 585.65(m), 614.20(m), 625.72(w) 702.36(s), 729.68(s), 757.82(s), 804.82(s), 850.14(m), 961.86(m), 1010.26(s), 1033.17(m), 1062.13(w), 1099.08(w), 1162.59 (s), 1271.47(m), 1380.77(w), 1426.64(m), 1461.62(s), 1478.56(m), 1592.19(s), 1650.76(m), 3052.87(w).

Table S1 Crystallographic data for complexes **1** and **2**.

Compound	**1**	**2**
Formula	$C_{71}H_{72}BDyF_2N_6O_4$	$C_{72}H_{72}BDyF_2N_6O_3$
Mr	1284.65	1280.66
Temperature/K	180.0	180.0
Crystal system	Monoclinic	Monoclinic
Space group	$P2_1$	$P2_1$
a/Å	16.7090(5)	16.7039(4)
b/Å	23.6685(7)	23.7837(7)
c/Å	20.7456(6)	20.8456(6)
□/°	90	90
□/°	96.2300(10)	96.1420(10)
□/°	90	90
Volume/Å^3	8156.0(4)	8237.6(4)
Z	4	4
ρcalc/g·cm^{-3}	1.046	1.033
F(000)	2644.0	2636.0
Crystal size/mm^3	0.21 × 0.14 × 0.12	0.2 × 0.15 × 0.13
Reflections collected	83334	84217
R_{int}	0.0542	0.0384
GOF on F^2	1.014	1.036
*R_1, wR_2 [I > = 2σ (I)]	0.0456, 0.1131	0.0371, 0.0921
*R_1, wR_2 [all data]	0.0536, 0.1179	0.0411, 0.0945
CCDC	2142837	2142838

*R_1 = S||*Fo*| − |*Fc*||/S|*Fo*| for *Fo* > 2s(*Fo*); wR_2 = (S*w*(*Fo*^{2} − *Fc*^{2})^2/S(*wFc*^{2})^2)$^{1/2}$ all reflections, *w* =1/[s^2(*Fo*^{2})+(0.1557P)^2] where P = (*Fo*^{2}+2*Fc*^{2})/3

Table S2 The CShM values calculated by SHAPE 2.1 for **1**.

Central atom	Coordination Geometry	**Dy1**	**Dy2**
Dy	Johnson triangular cupola J3 (C_{3v})	14.576	14.233
	Capped cube J8 (C_{4v})	6.591	6.995
	Spherical-relaxed capped cube (C_{4v})	5.886	6.099
	Capped square antiprism J10 (C_{4v})	7.036	7.244
	Spherical capped square antiprism (C_{4v})	6.067	6.259
	Tricapped trigonal prism J51 (D_{3h})	6.107	6.520
	Spherical tricapped trigonal prism (D_{3h})	7.044	7.418
	Tridiminished icosahedron J63 (C_{3v})	11.345	11.533
	Hula-hoop (D_{2v})	3.394	3.386
	Muffin (C_s)	4.731	4.851

Table S3 The CShM values calculated by SHAPE 2.1 for **2**.

Central atom	Coordination Geometry	**Dy1**	**Dy2**
Dy	Johnson triangular cupola J3 (C_{3v})	14.424	14.253
	Capped cube J8 (C_{4v})	6.601	6.746
	Spherical-relaxed capped cube (C_{4v})	5.855	5.818
	Capped square antiprism J10 (C_{4v})	7.090	7.362
	Spherical capped square antiprism (C_{4v})	6.091	6.402
	Tricapped trigonal prism J51 (D_{3h})	6.115	6.612
	Spherical tricapped trigonal prism (D_{3h})	7.002	7.507
	Tridiminished icosahedron J63 (C_{3v})	11.057	11.707
	Hula-hoop (D_{2v})	3.292	3.216
	Muffin (C_s)	4.786	4.939

Table S4 Selected bond distances (Å) for **1**.

Dy1	Dy2
Dy1−F1 2.144(9)	Dy2−F3 2.157(10)
Dy1−F2 2.218(9)	Dy2−F4 2.159(8)
Dy1−O1 2.339(11)	Dy2−O2 2.397(9)
Dy1−N1 2.602(10)	Dy2−N7 2.597(11)
Dy1−N2 2.649(12)	Dy2−N8 2.726(11)
Dy1−N3 2.600(11)	Dy2−N9 2.630(11)
Dy1−N4 2.636(11)	Dy2−N10 2.609(11)
Dy1−N5 2.727(11)	Dy2−N11 2.674(12)
Dy1−N6 2.654(11)	Dy2−N12 2.631(12)
Dy−Naverage 2.645	Dy−Naverage 2.646

Table S5 Selected bond distances (Å) for **2**.

Dy1	Dy2
Dy1−F1 2.161(7)	Dy2−F3 2.157(8)
Dy1−F2 2.228(8)	Dy2−F4 2.157(7)
Dy1−O1 2.325(8)	Dy2−O2 2.406(11)
Dy1−N1 2.608(10)	Dy2−N7 2.612(9)
Dy1−N2 2.650(10)	Dy2−N8 2.693(10)
Dy1−N3 2.616(9)	Dy2−N9 2.637(10)
Dy1−N4 2.632(10)	Dy2−N10 2.620(9)
Dy1−N5 2.726(9)	Dy2−N11 2.677(10)
Dy1−N6 2.649(9)	Dy2−N12 2.655(10)
Dy−Naverage 2.647	Dy−Naverage 2.649

Table S6 Selected bond angles (°) for **1**.

Dy1	Dy2
F1−Dy1−F2 145.6(4)	F3−Dy2−F4 146.4(4)
F1-Dy1-O1 143.8(4)	F3-Dy2-O2 144.1(4)
F2-Dy1-O1 70.4(3)	F4-Dy2-O2 69.5(4)
F1−Dy1−N1 89.3(3)	F3−Dy2−N7 98.5(4)
F1−Dy1−N2 90.2(4)	F3−Dy2−N8 75.3(4)
F1−Dy1−N3 79.8(4)	F3−Dy2−N9 76.9(4)
F1−Dy1−N4 99.4(4)	F3−Dy2−N10 91.3(4)
F1−Dy1−N5 75.7(4)	F3−Dy2−N11 75.6(4)
F1−Dy1−N6 78.2(4)	F3−Dy2−N12 81.3(4)
F2−Dy1−N1 83.8(4)	F4−Dy2−N7 79.2(4)
F2−Dy1−N2 70.6(4)	F4−Dy2−N8 74.4(4)
F2−Dy1−N3 75.4(4)	F4−Dy2−N9 75.7(3)
F2−Dy1−N4 89.3(4)	F4−Dy2−N10 92.7(4)
F2−Dy1−N5 135.5(4)	F4−Dy2−N11 134.4(4)
F2−Dy1−N6 126.3(4)	F4−Dy2−N12 123.8(4)
N1−Dy1−N2 61.7(3)	N7−Dy2−N8 61.0(4)
N1−Dy1−N3 123.0(3)	N7−Dy2−N9 120.4(4)
N1−Dy1−N4 170.2(4)	N7−Dy2−N10 170.3(4)
N1−Dy1−N5 121.4(3)	N7−Dy2−N11 121.2(4)
N1−Dy1−N6 61.4(3)	N7−Dy2−N12 60.8(3)
N2−Dy1−N3 61.3(3)	N8−Dy2−N9 60.5(4)
N2−Dy1−N4 122.4(4)	N8−Dy2−N10 122.2(4)
N2−Dy1−N5 152.2(4)	N8−Dy2−N11 150.8(4)
N2−Dy1−N6 116.7(4)	N8−Dy2−N12 111.9(4)
N3−Dy1−N4 61.5(3)	N9−Dy2−N10 61.7(4)
N3−Dy1−N5 110.1(4)	N9−Dy2−N11 114.9(4)
N3−Dy1−N6 157.7(4)	N9−Dy2−N12 158.1(4)
N4−Dy1−N5 59.9(4)	N10−Dy2−N11 61.3(4)
N4−Dy1−N6 118.5(4)	N10−Dy2−N12 121.3(4)
N5−Dy1−N6 60.1(3)	N11−Dy2−N12 60.4(3)

Table S7 Selected bond angles (°) for **2**.

Dy1	Dy2
F1−Dy1−F2 145.1(3)	F3−Dy2−F4 145.4(4)
F1-Dy1-O1 143.9(3)	F3-Dy2-O2 143.6(3)
F2-Dy1-O1 76.3(3)	F4-Dy2-O2 70.9(3)
F1−Dy1−N1 89.3(3)	F3−Dy2−N7 98.7(3)
F1−Dy1−N2 76.8(3)	F3−Dy2−N8 72.9(3)
F1−Dy1−N3 79.8(3)	F3−Dy2−N9 78.7(3)
F1−Dy1−N4 99.6(3)	F3−Dy2−N10 91.3(3)
F1−Dy1−N5 76.0(3)	F3−Dy2−N11 75.3(3)
F1−Dy1−N6 77.6(3)	F3−Dy2−N12 81.9(3)
F2−Dy1−N1 83.1(3)	F4−Dy2−N7 78.9(3)
F2−Dy1−N2 69.5(3)	F4−Dy2−N8 72.9(3)
F2−Dy1−N3 76.1(3)	F4−Dy2−N9 73.2(3)
F2−Dy1−N4 90.4(4)	F4−Dy2−N10 92.6(3)
F2−Dy1−N5 136.2(3)	F4−Dy2−N11 135.5(3)
F2−Dy1−N6 126.0(3)	F4−Dy2−N12 124.0(3)
N1−Dy1−N2 61.9(3)	N7−Dy2−N8 60.7(3)
N1−Dy1−N3 123.2(3)	N7−Dy2−N9 119.9(3)
N1−Dy1−N4 170.9(3)	N7−Dy2−N10 170.0(3)
N1−Dy1−N5 121.4(3)	N7−Dy2−N11 121.6(3)
N1−Dy1−N6 61.1(3)	N7−Dy2−N12 61.1(3)
N2−Dy1−N3 61.3(3)	N8−Dy2−N9 60.6(3)
N2−Dy1−N4 121.7(3)	N8−Dy2−N10 122.1(3)
N2−Dy1−N5 152.5(3)	N8−Dy2−N11 151.1(3)
N2−Dy1−N6 116.9(3)	N8−Dy2−N12 112.5(3)
N3−Dy1−N4 60.8(3)	N9−Dy2−N10 61.5(3)
N3−Dy1−N5 109.7(3)	N9−Dy2−N11 115.6(3)
N3−Dy1−N6 157.0(3)	N9−Dy2−N12 160.5(2)
N4−Dy1−N5 60.0(3)	N10−Dy2−N11 61.5(3)
N4−Dy1−N6 118.9(3)	N10−Dy2−N12 121.3(3)
N5−Dy1−N6 60.3(3)	N11−Dy2−N12 60.5(3)

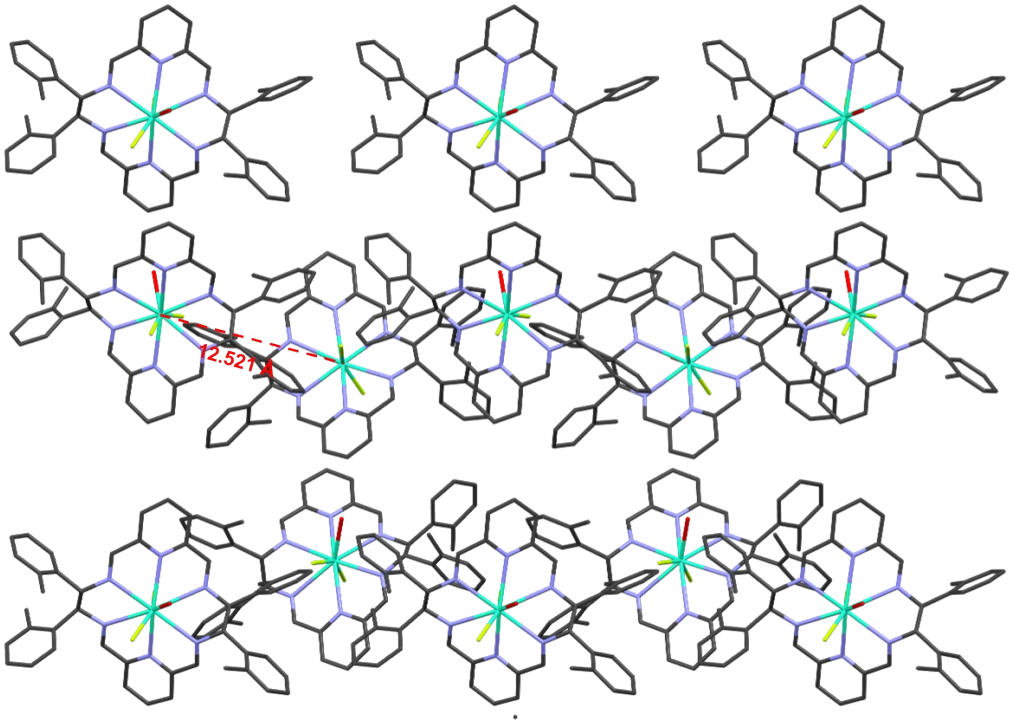

Fig. S1 The packing diagram for **1** gives the shortest intermolecular Dy···Dy distance of 12.521 Å.

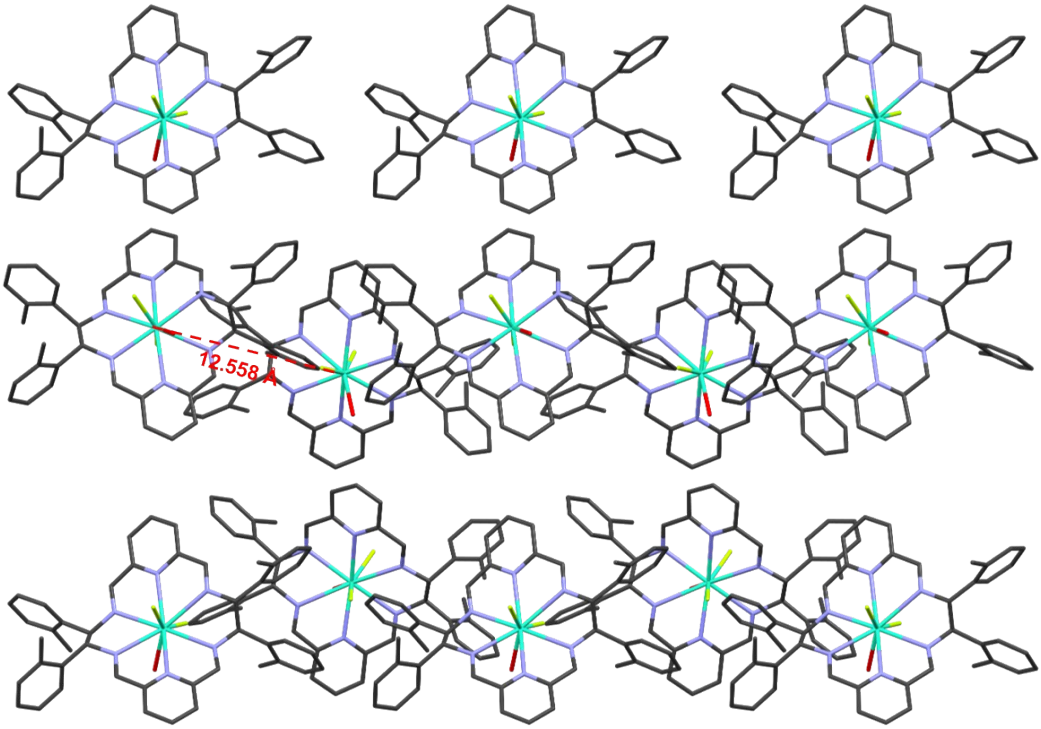

Fig. S2 The packing diagram for **2** gives the shortest intermolecular Dy···Dy distance of 12.558 Å.

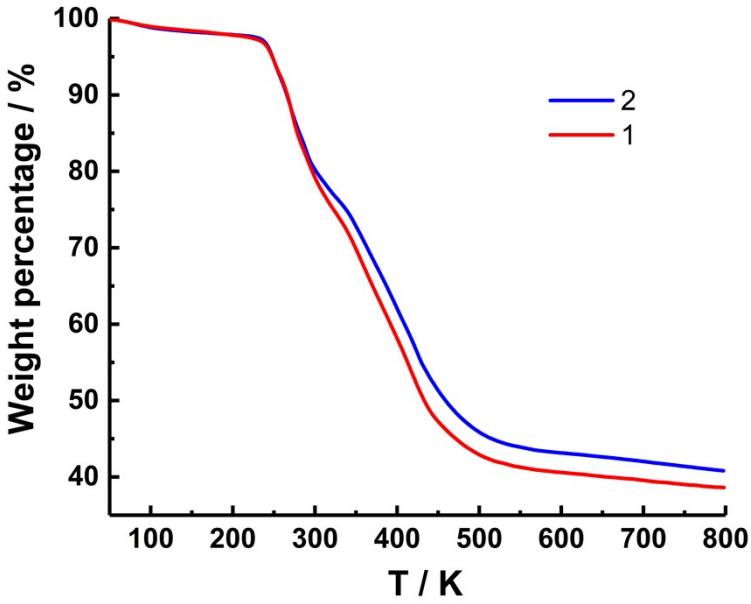

Fig. S3 Thermogravimetric analysis of **1** (red line) and **2** (blue line).

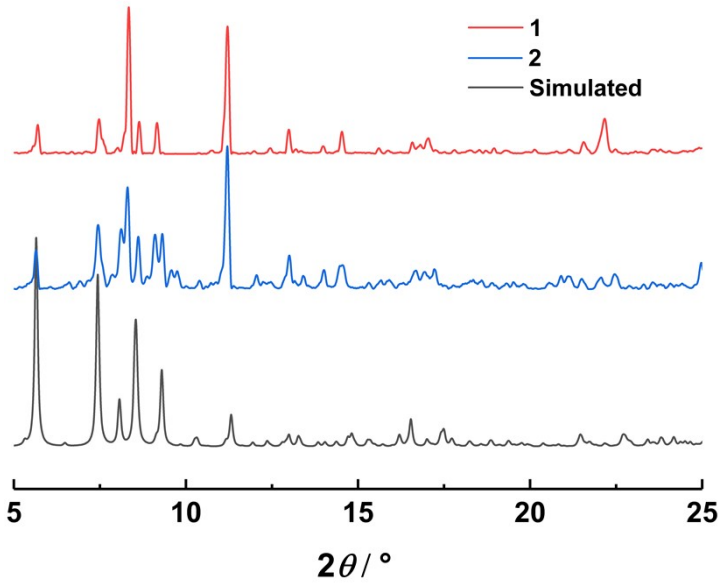

Fig. S4 Powder XRD analyses of **1** (red line) and **2** (blue line). The black line is simulated data from single crystal data.

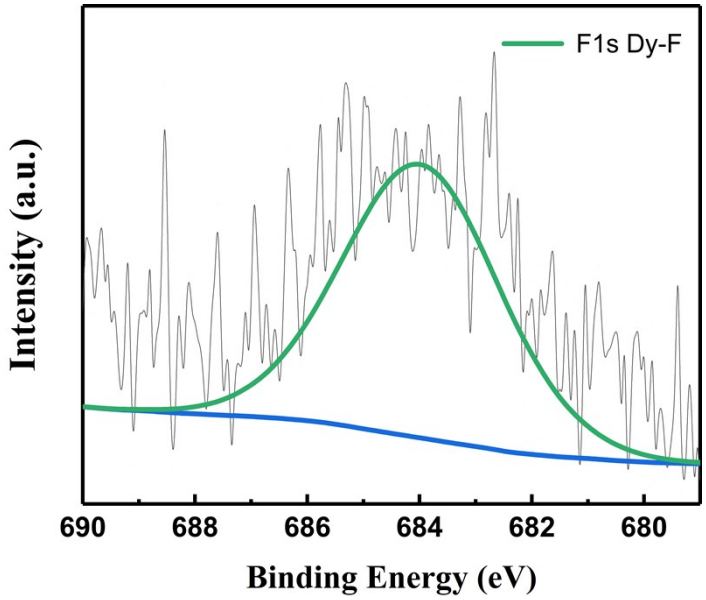

Fig. S5 X-ray photoelectron spectrum of F1s for **1**.

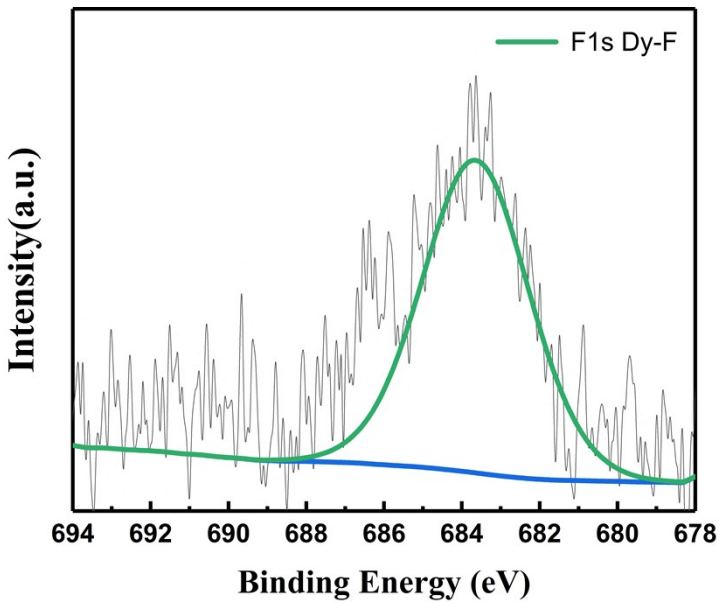

Fig. S6 X-ray photoelectron spectrum of F1s for **2**.

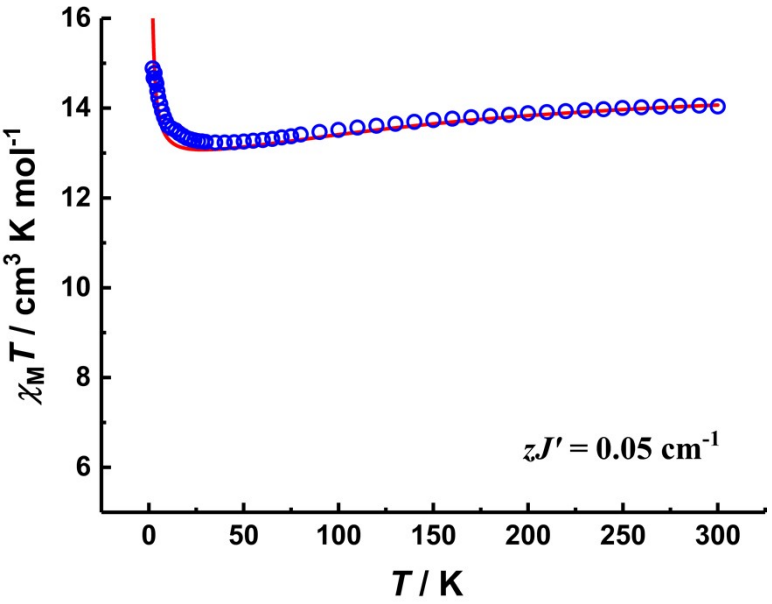

Fig. S7 Calculated (red solid line) and experimental (blue circle) data of magnetic susceptibilities of **1**. The intermolecular interaction parameters *zJ´* of **1** was fitted to 0.05 cm^{-1}.

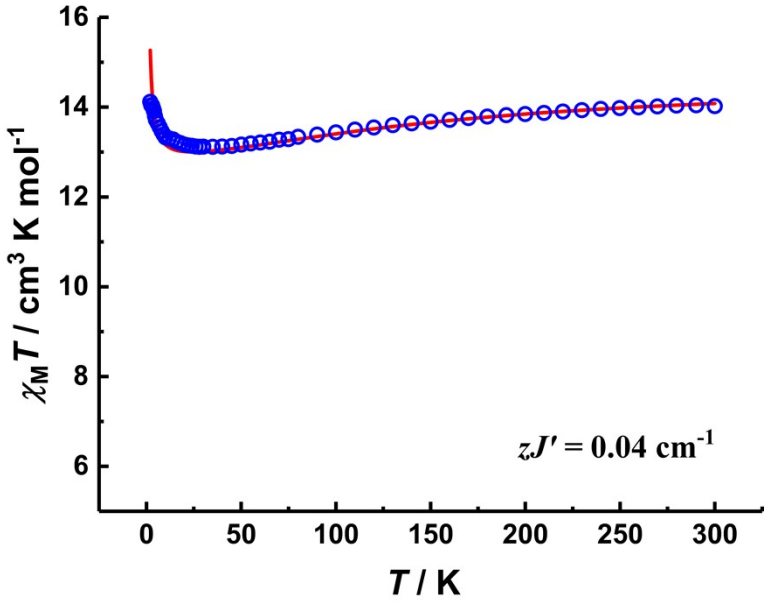

Fig. S8 Calculated (red solid line) and experimental (blue circle) data of magnetic susceptibilities of **2**. The intermolecular interaction parameters *zJ´* of **2** was fitted to 0.04 cm^{-1}.

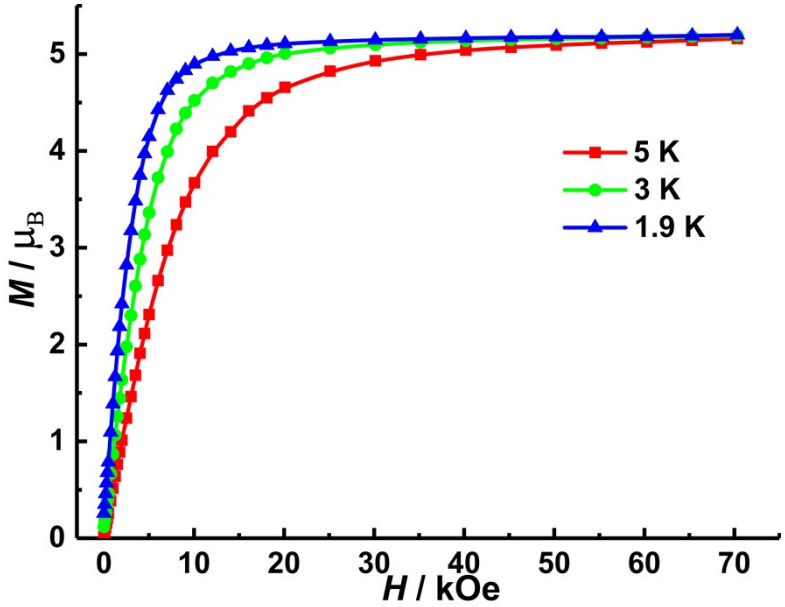

Fig. S9 Field dependence of the magnetization at 1.9, 3 and 5 K for **1**.

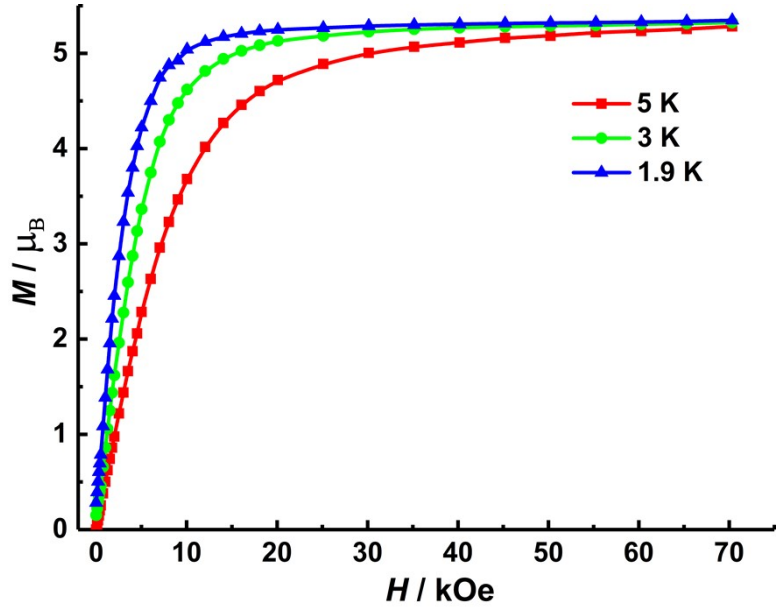

Fig. S10 Field dependence of the magnetization at 1.9, 3 and 5 K for **2**.

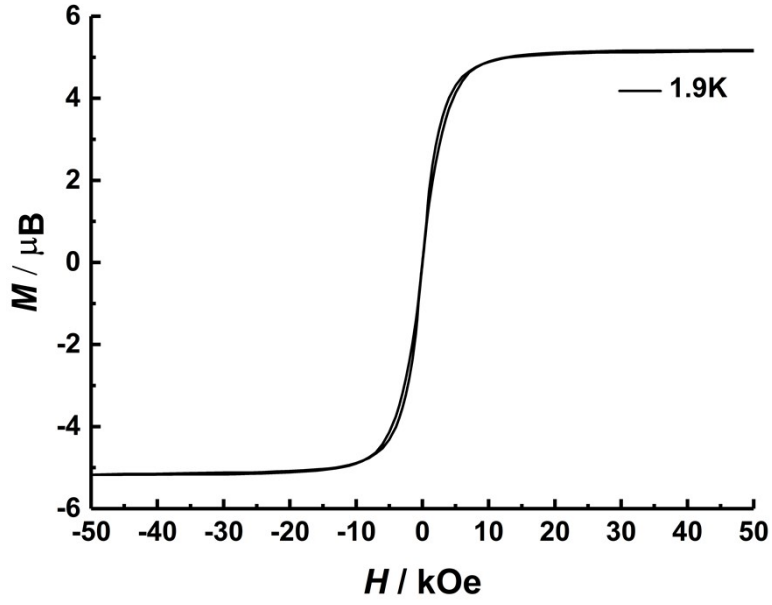

Fig. S11 *M*(*H*) hysteresis loops for **1** at 1.9 K using an average sweep rate of 42 Oe/s.

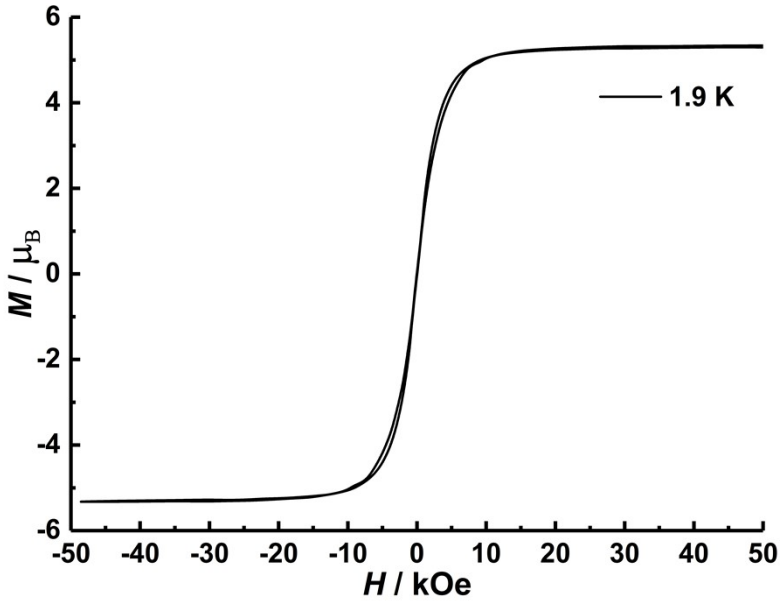

Fig. S12 *M*(*H*) hysteresis loops for **2** at 1.9 K using an average sweep rate of 31 Oe/s.

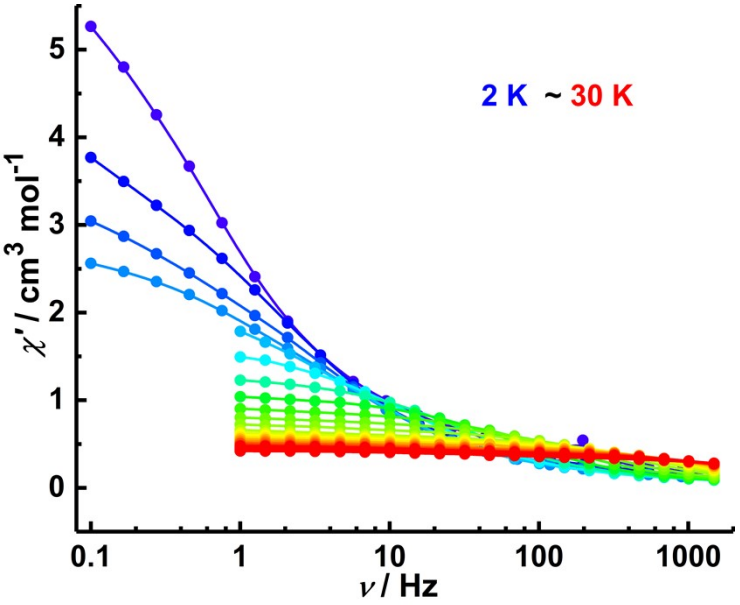

Fig. S13 Frequency dependence of the in-phase ac susceptibility component under a zero applied dc field for **1**.

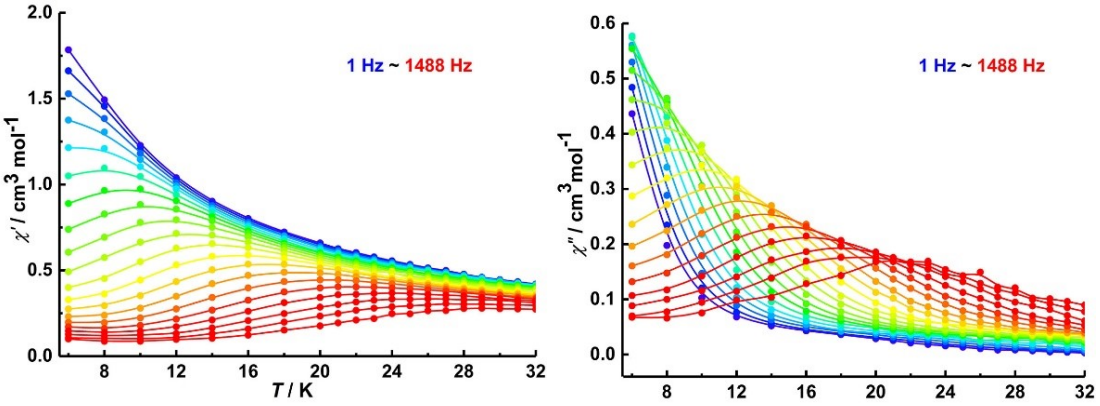

Fig. S14 Temperature dependence of the in-phase (left) and out-of-phase (right) ac susceptibility component under a zero applied dc field for **1**.

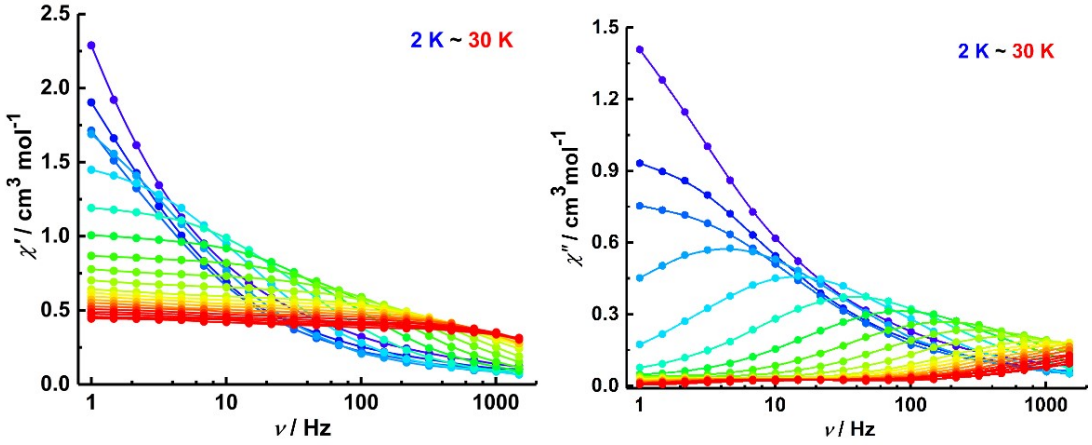

Fig. S15 Frequency dependence of the in-phase (left) and out-of-phase (right) ac susceptibility component under a zero applied dc field for **2**.

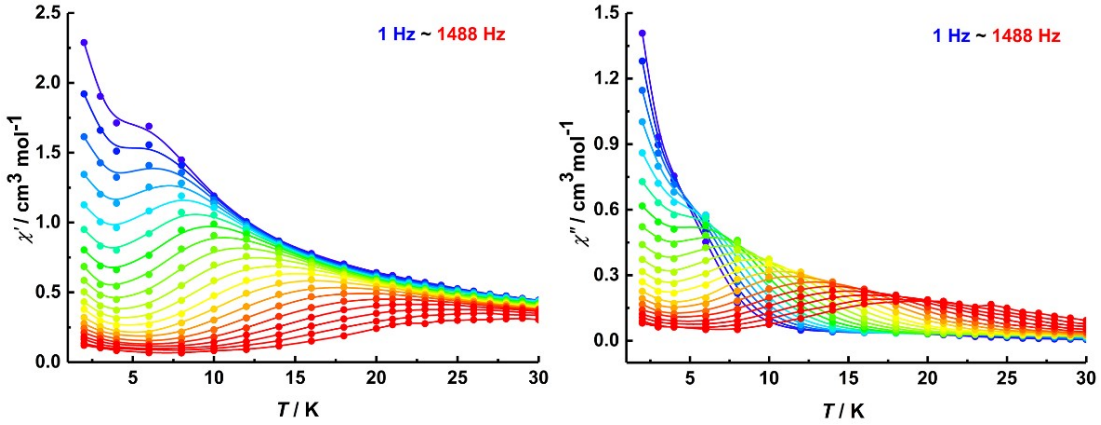

Fig. S16 Temperature dependence of the in-phase (left) and out-of-phase (right) ac susceptibility component under a zero applied dc field for **2**.

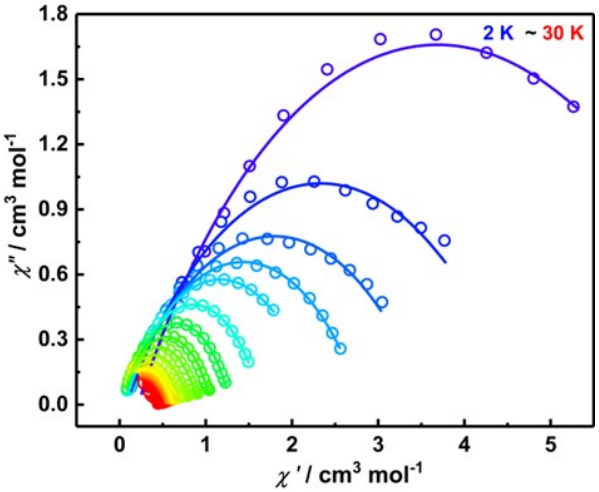

Fig. S17 Cole-Cole plots under zero-dc field for **1**. The solid lines are best fits to the Debye's law.

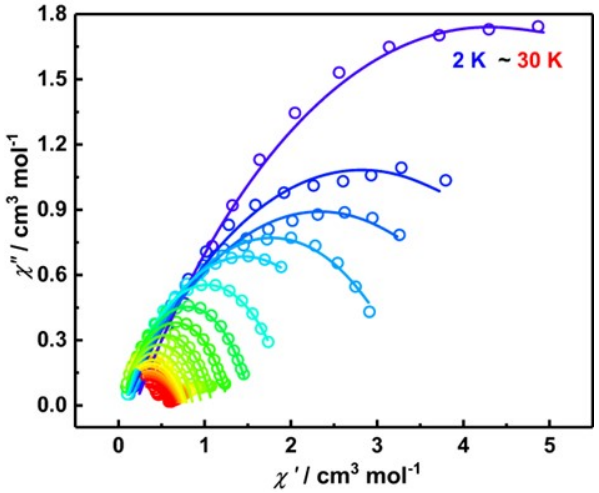

Fig. S18 Cole-Cole plots under zero-dc field for **2**. The solid lines are best fits to the Debye's law.

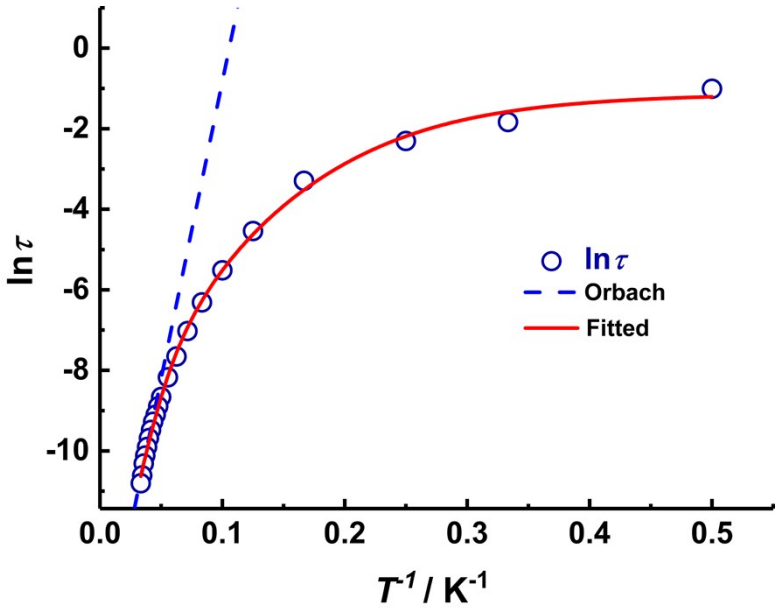

Fig. S19 Temperature dependence of the relaxation time in the form of natural logarithm for **2**. The red line is given by $\ln\tau = -\ln[CT^n + \tau_0^{-1}\exp(-U_{eff}/k_BT) + \tau_{QTM}^{-1}]$.

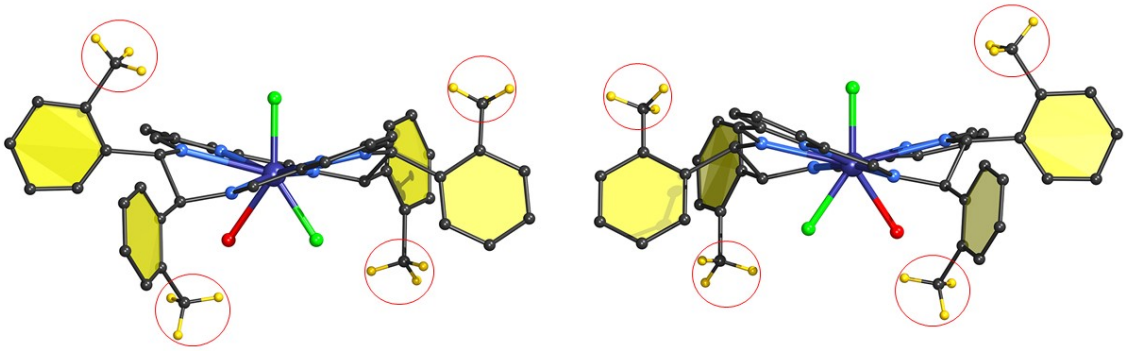

Fig. S20 Molecular structures of complexes SSSS-Dy-2-Me (**1**) (left) and RRRR-Dy-2-Me (**2**) (right), emphasizing the methyl of steric hindrance.

Computational details

Complexes **1** and **2** are both mononuclear, but each of them includes two types of molecular structures. Complete-active-space self-consistent field (CASSCF) calculations on two types of molecular structures indicated as **1_Dy1**, **1_Dy2**, **2_Dy1** and **2_Dy2** for complexes **1** and **2** (see Fig. S18) on the basis of single-crystal X-ray determined geometry have been carried out with OpenMolcas[5] program package.

The basis sets for all atoms are atomic natural orbitals from the ANO-RCC library: ANO-RCC-VTZP for Dy^{III}; VTZ for close N, O and F; VDZ for distant atoms. The calculations employed the second order Douglas-Kroll-Hess Hamiltonian, where scalar relativistic contractions were taken into account in the basis set and the spin-orbit couplings were handled separately in the restricted active space state interaction (RASSI-SO) procedure.[6, 7] Active electrons in 7 active orbitals include all *f* electrons (CAS(9 in 7 for Dy^{III})) in the CASSCF calculation. To exclude all the doubts, we calculated all the roots in the active space. We have mixed the maximum number of spin-free state which was possible with our hardware (all from 21 sextets, 128 from 224 quadruplets, 130 from 490 doublets) for each complex. SINGLE_ANISO[8-10] program was used to obtain the energy levels, ***g*** tensors, magnetic axes, *et al.* based on the above CASSCF/RASSI-SO calculations. The intermolecular exchange interaction for **1** and **2** was modeled in the POLY-ANISO module of OpenMolcas.[11-13]

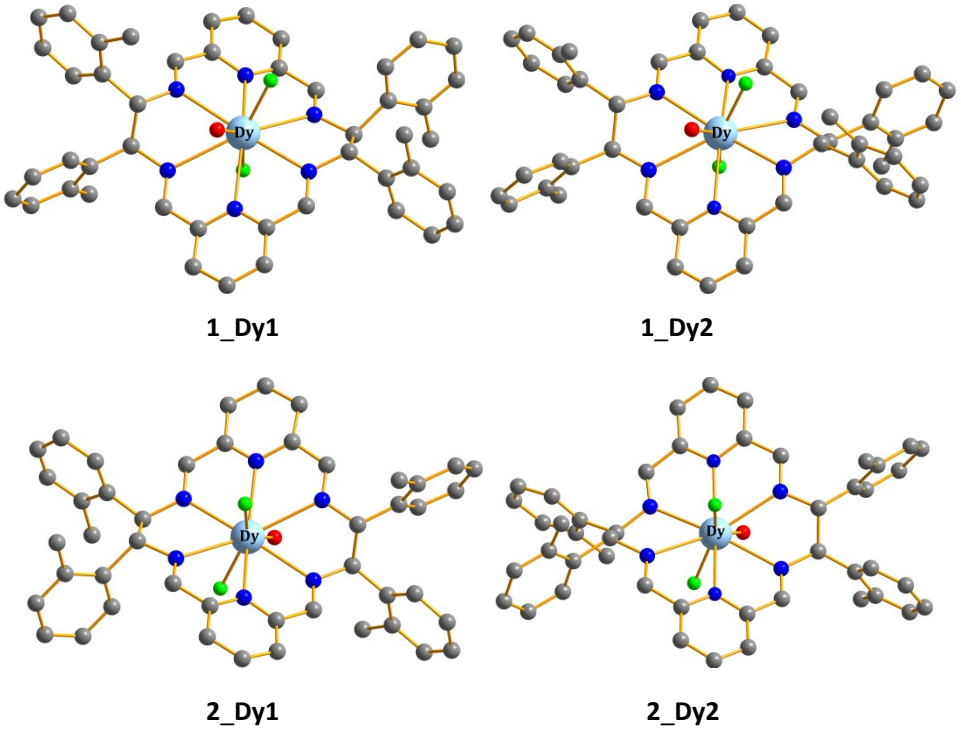

Fig. S21 Calculated two types of molecular structures for each of complexes **1** and **2**; H atoms are omitted for clarify.

Table S8 Weight of calculated crystal-field parameters *B(k,q)* of complexes **1** and **2**.

k	*q*	**1_Dy1**	**1_Dy2**	**2_Dy1**	**2_Dy2**
	–2	8.70%	1.04%	8.64%	0.96%
	–1	3.51%	3.30%	0.53%	3.16%
2	0	26.89%	39.23%	28.75%	37.79%
	1	0.97%	3.31%	3.22%	2.84%
	2	2.35%	6.01%	0.17%	6.16%
	–4	0.97%	0.12%	1.57%	0.02%
	–3	0.27%	1.75%	3.18%	2.45%
	–2	6.99%	1.81%	7.67%	1.55%
	–1	2.07%	1.11%	0.41%	1.03%
4	0	8.36%	9.01%	8.17%	7.71%
	1	0.88%	1.71%	2.35%	1.21%
	2	1.61%	6.44%	1.67%	7.40%
	3	2.91%	1.79%	0.68%	2.18%
	4	0.42%	0.90%	1.08%	1.21%
	–6	0.63%	0.16%	0.24%	1.95%
	–5	6.21%	3.39%	0.72%	3.70%
	–4	0.34%	1.63%	0.17%	1.78%
	–3	0.04%	0.81%	2.16%	0.47%
	–2	0.15%	0.02%	0.61%	0.02%
	–1	2.90%	1.52%	1.15%	1.49%
6	0	2.66%	2.71%	1.95%	2.35%
	1	1.44%	0.30%	2.28%	0.41%
	2	1.29%	0.89%	0.98%	0.89%
	3	1.90%	1.02%	0.16%	1.40%
	4	1.32%	0.24%	1.69%	0.05%
	5	1.06%	0.62%	6.77%	1.27%
	6	9.86%	7.41%	9.72%	6.88%

Table S9 Calculated energy levels (cm^{-1}), ***g*** (g_x, g_y, g_z) tensors and predominant m_J values of the lowest eight Kramers doublets (KDs) for complexes **1** and **2** using CASSCF/RASSI-SO with OpenMolcas.

KDs	**1_Dy1**			**1_Dy2**		
	E/cm^{-1}	***g***	m_J	E/cm^{-1}	***g***	m_J
1	0.0	0.006 0.007 19.815	±15/2	0.0	0.004 0.004 19.846	±15/2
2	328.6	0.066 0.088 16.911	±13/2	369.3	0.073 0.087 16.966	±13/2
3	597.7	0.617 0.738 13.695	±11/2	676.5	0.170 0.196 13.961	±11/2
4	771.9	5.659 6.236 8.284	±9/2	883.4	4.160 4.564 9.549	±9/2
5	896.8	1.979 3.853 9.411	±7/2	1000.1	3.138 4.337 12.400	±7/2
6	918.4	1.688 5.190 13.853	±1/2	1057.4	0.892 1.912 14.053	±1/2
7	996.6	0.034 0.096 17.830	±3/2	1082.6	0.146 1.063 11.838	±3/2
8	1101.6	0.044 0.145 18.710	±5/2	1152.5	0.030 0.904 17.151	±5/2
KDs	**2_Dy1**			**2_Dy2**		
	E/cm^{-1}	***g***	m_J	E/cm^{-1}	***g***	m_J
1	0.0	0.005 0.006 19.816	±15/2	0.0	0.005 0.006 19.829	±15/2
2	346.9	0.078 0.103 16.892	±13/2	334.2	0.077 0.092 16.947	±13/2
3	622.7	0.518 0.634 13.754	±11/2	617.4	0.241 0.280 13.947	±11/2
4	807.4	5.286 5.697 8.803	±9/2	814.1	4.231 4.373 9.662	±9/2
5	943.7	1.529 4.037 10.113	±7/2	932.4	3.359 4.115 12.041	±7/2
6	996.5	1.375 2.331 15.196	±1/2	994.9	0.741 2.880 13.448	±1/2
7	1052.3	0.015 0.084 17.158	±3/2	1021.1	1.079 4.040 11.960	±3/2

8	1137.8	0.008 0.112 18.385	±5/2	1078.4	0.138 0.190 16.869	±5/2

Table S10 Wave functions with definite projection of the total moment | m_J > for the lowest eight KDs of complexes **1** and **2** using CASSCF/RASSI-SO with OpenMolcas.

	E/cm^{-1}	wave functions
1_Dy1	0.0	98.9%|±15/2>
	328.6	95.3%|±13/2>
	597.7	84.6%|±11/2>+7.0%|±7/2>
	771.9	59.8%|±9/2>+15.2%|±5/2>+9.0%|±3/2>+8.8%|±7/2>
	896.8	46.2%|±7/2>+17.6%|±3/2>+15.5%|±9/2>+9.0%|±5/2>+8.3%|±1/2>
	918.4	38.8%|±1/2>+28.9%|±5/2>+16.8%|±3/2>+7.7%|±7/2>
	996.6	35.9%|±3/2>+35.8%|±1/2>+17.0%|±5/2>+6.3%|±7/2>
	1101.6	29.5%|±5/2>+23.9%|±7/2>+20.4%|±3/2>+14.0%|±1/2>+9.7%|±9/2>
1_Dy2	0.0	99.4%|±15/2>
	369.3	97.3%|±13/2>
	676.5	90.2%|±11/2>
	883.4	69.8%|±9/2>+9.1%|±5/2>+8.5%|±3/2>+7.4%|±7/2>
	1000.1	52.0%|±7/2>+27.0%|±5/2>+13.1%|±9/2>+4.7%|±3/2>
	1057.4	68.9%|±1/2>+16.0%|±3/2>+10.2%|±5/2>
	1082.6	54.7%|±3/2>+21.6%|±1/2>+12.9%|±5/2>+5.1%|±7/2>
	1152.5	40.7%|±5/2>+29.1%|±7/2>+15.8%|±3/2>+7.0%|±9/2>
2_Dy1	0.0	98.9%|±15/2>
	346.9	95.0%|±13/2>
	622.7	84.1%|±11/2>+7.8%|±7/2>
	807.4	60.8%|±9/2>+16.1%|±5/2>+7.7%|±3/2>+6.9%|±7/2>
	943.7	48.9%|±7/2>+21.0%|±9/2>+14.3%|±3/2>+8.6%|±5/2>
	996.5	46.3%|±1/2>+27.1%|±5/2>+14.9%|±3/2>+9.7%|±7/2>
	1052.3	41.3%|±3/2>+30.2%|±1/2>+19.8%|±5/2>+5.1%|±7/2>
	1137.8	28.0%|±5/2>+21.6%|±7/2>+21.5%|±3/2>+18.0%|±1/2>+8.6%|±9/2>
2_Dy2	0.0	99.2%|±15/2>
	334.2	96.7%|±13/2>
	617.4	89.4%|±11/2>+4.4%|±7/2>
	814.1	71.2%|±9/2>+9.3%|±5/2>+7.5%|±3/2>+6.6%|±7/2
	932.4	56.1%|±7/2>+23.2%|±5/2>+12.9%|±9/2>
	994.9	49.5%|±1/2>+25.3%|±3/2>+19.0%|±5/2>
	1021.1	45.1%|±3/2>+38.3%|±1/2>+10.1%|±5/2>
	1078.4	38.2%|±5/2>+26.2%|±7/2>+18.4%|±3/2>+8.2%|±1/2>

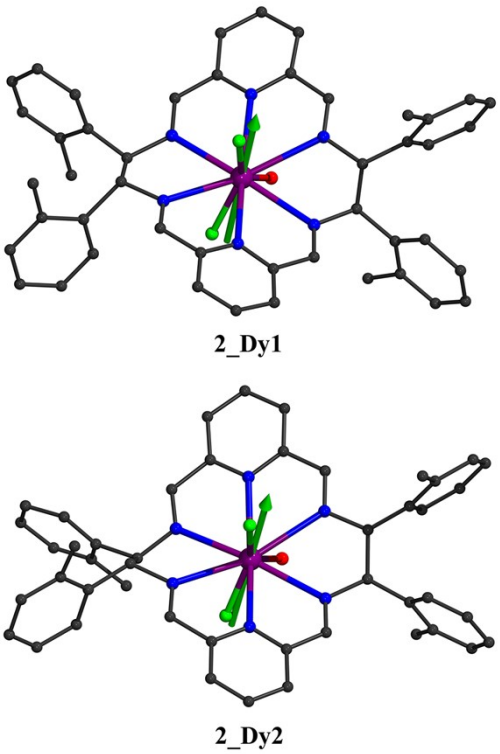

Fig. S22 Calculated orientations of the local main magnetic axes on Dy^{III} ions of complex **2** in their ground KDs.

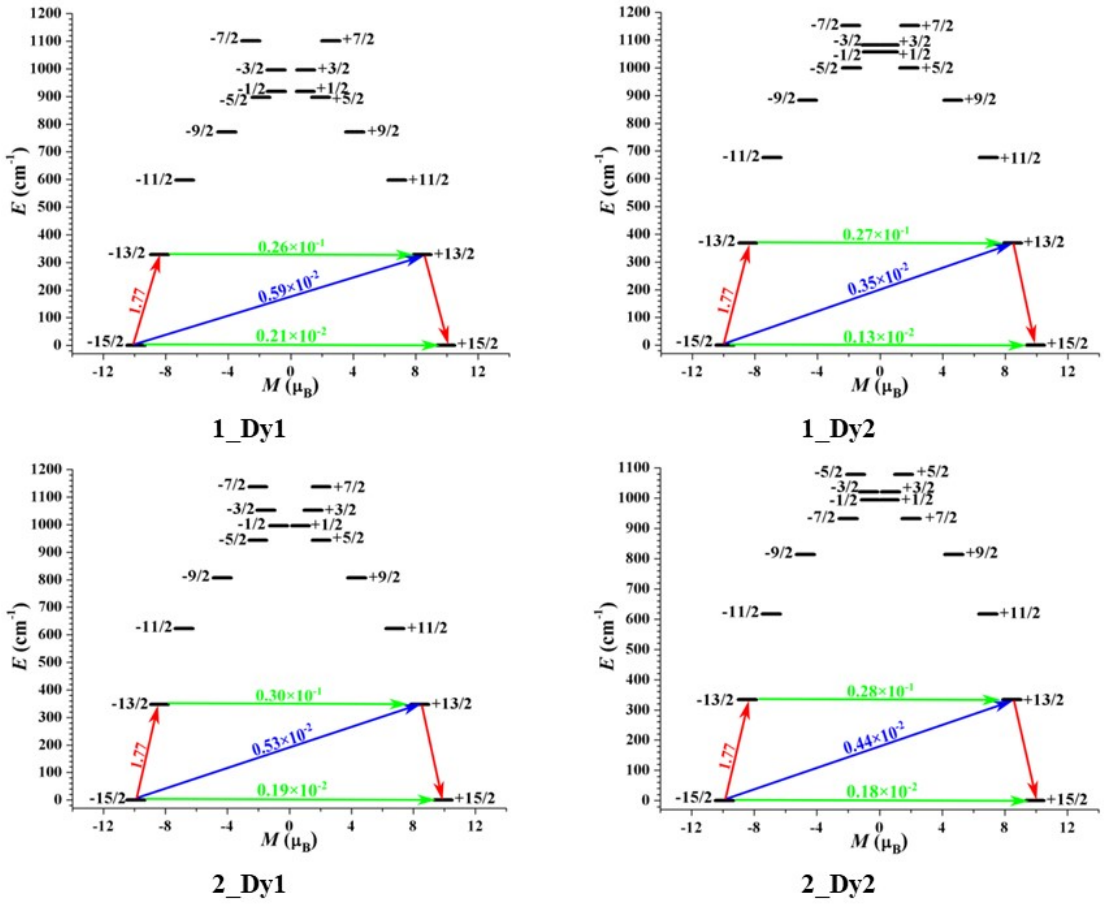

Fig. S23 Magnetization blocking barriers of complexes **1** and **2**. The thick black lines represent the KDs of the individual molecular structures as a function of their magnetic moment along the magnetic axis. The green lines correspond to diagonal matrix element of the transversal magnetic moment; the blue lines represent Orbach relaxation processes. The path shown by the red arrows represents the most probable path for magnetic relaxation in the corresponding compounds. The numbers at each arrow stand for the mean absolute value of the corresponding matrix element of transition magnetic moment.

1. M. Zhou, K. Li, D. Chen, R. Xu, G. Xu and W. Tang, *J. Am. Chem. Soc.*, 2020, **142**, 10337-10342.
2. G. Sheldrick, *Acta Crystallogr. Sect. A*, 2015, **71**, 3-8.
3. G. Sheldrick, *Acta Crystallogr. Sect. C-Struct. Chem.*, 2015, **71**, 3-8.
4. O. V. Dolomanov, L. J. Bourhis, R. J. Gildea, J. A. K. Howard and H. Puschmann, *J. Appl. Crystallogr.*, 2009, **42**, 339-341.
5. I. Fdez. Galván, M. Vacher, A. Alavi, C. Angeli, F. Aquilante, J. Autschbach, J. J. Bao, S. I. Bokarev, N. A. Bogdanov, R. K. Carlson, L. F. Chibotaru, J. Creutzberg, N. Dattani, M. G. Delcey, S. S. Dong, A. Dreuw, L. Freitag, L. M. Frutos, L. Gagliardi, F. Gendron, A. Giussani, L. González, G. Grell, M. Guo, C. E. Hoyer, M. Johansson, S. Keller, S. Knecht, G. Kovačević, E. Källman, G. Li Manni, M. Lundberg, Y. Ma, S. Mai, J. P. Malhado, P. Å. Malmqvist, P. Marquetand, S. A. Mewes, J. Norell, M. Olivucci, M. Oppel, Q. M. Phung, K. Pierloot, F. Plasser, M. Reiher, A. M. Sand, I. Schapiro, P. Sharma, C. J. Stein, L. K. Sørensen, D. G. Truhlar, M. Ugandi, L. Ungur, A. Valentini, S. Vancoillie, V. Veryazov, O. Weser, T. A. Wesołowski, P.-O. Widmark, S. Wouters, A. Zech, J. P. Zobel and R. Lindh, *J. Chem. Theory Comput.*, 2019, **15**, 5925-5964.
6. P. Å. Malmqvist, B. O. Roos and B. Schimmelpfennig, *Chem. Phys. Lett.*, 2002, **357**, 230-240.
7. B. A. Heß, C. M. Marian, U. Wahlgren and O. Gropen, *Chem. Phys. Lett.*, 1996, **251**, 365-371.
8. L. F. Chibotaru, L. Ungur and A. Soncini, *Angew. Chem. Int. Ed.*, 2008, **47**, 4126-4129.
9. L. Ungur, W. Van den Heuvel and L. F. Chibotaru, *New J. Chem.*, 2009, **33**, 1224-1230.
10. L. F. Chibotaru, L. Ungur, C. Aronica, H. Elmoll, G. Pilet and D. Luneau, *J. Am. Chem. Soc.*, 2008, **130**, 12445-12455.
11. M. E. Lines, *J. Chem. Phys.*, 1971, **55**, 2977-2984.
12. L. F. Chibotaru, L. Ungur and A. Soncini, *Angew. Chem. Int. Ed.*, 2008, **47**, 4126-4129.
13. L. Ungur and L. F. Chibotaru, Computational Modelling of the Magnetic Properties of Lanthanide Compounds. in *Lanthanides and Actinides in Molecular Magnetism*, Wiley-VCH Verlag GmbH & Co. KGaA, 2015.